Dynamical simulations of phonon dynamics in ultra-cold ion crystals

D. Meiser
Tech-X Corporation, 5261 Arapahoe Ave. Ste A, Boulder, Colorado 80303, USA.

J. Britton, B. Sawyer, and J. J. Bollinger
NIST Boulder

I. INTRODUCTION

Ultra-cold ions in Penning traps are an extremely powerful experimental platform for research in quantum information science and quantum computing [**?**] and quantum information, quantum simulation, and quantum metrology. These systems have been used to simulated complex, strongly correlated condensed matter systems and quantum magnetic systems [**?**].

`Also mention plasma physics problems that can be studied. Very strongly correlated plasma.`

Successful experiments in these areas critically depend on laser cooling of the ions to near their motional ground state. At these temperatures the ions form a crystal that is the basis of e.g. the quantum simulation experiments. The next generation of experiments requires colder temperatures (or rather more stable crystals). That would allow single site state preparation and single site readout, perhaps doing quantum computation in Penning traps with much larger numbers of ions than what's possible in Paul traps.

Simulation can provide very useful insight into the thermal ion dynamics, rearrangements of the ions in the crystal, and the interplay between these phenomena and the laser cooling and trap characteristics. `Discuss some of the stuff that the Freericks group has done with their simulations`

Here we present results from molecular dynamics simulations of the ion motion in a Penning trap including laser cooling. By including a microscopic model of the laser cooling that includes damping and recoil heating we are able to go beyond what's been done before. We get the temperature of the individual phonon modes and we can study the mobility of the ions on a per site basis. We can study the ion dynamics over a wider range of trap geometries (greater aspect ratio, multi-plane crystals, etc.). We can study the impact of misalignment of the cooling lasers and we can study the crystal stability as a function of the diameter of the cooling lasers. More complex cooling geometries (e.g. two counter-propagating cooling beams) can be studied easily, providing valuable insight for potential future improvements of the experiment.

Describe the major challenge in the theory of the laser cooling of th in-plane motion.

In this paper...

II. NUMERICAL INTEGRATION OF ION DYNAMICS

Our goal is a first principles, microscopic simulation of the ion dynamics. We have to account for the following forces acting on the ions: `More detailed description of Penning trap needed. Reference to Freericks paper`

- Cyclotron motion in the axial magnetic field of approximately 5T.
- Coulomb interactions between the ions.
- Electro-static trapping potential and rotating-wall potential.
- Laser cooling forces including damping and fluctuations.

In this section we describe our model for these forces and how we deal with them numerically.

A. Ion Hamiltonian

Some of the forces are easier to express in the lab frame and some of the forces are easier to describe in a frame of reference that is co-rotating with the rotating wall potential. We choose to describe the ion dynamics in the lab frame.

The Hamiltonian for the dynamics of the ions is

$$\hat{H}_{\rm tot} = \hat{H}_B + \hat{H}_\varphi + \hat{H}_L \ . \tag{1}$$

The Hamiltonian for motion in a magnetic field is

$$\hat{H}_B = \sum_{j=1}^{N} \frac{1}{2m_j} (\mathbf{p}_j - q_j \mathbf{A}(\mathbf{r_j}))^2 \ , \tag{2}$$

With m_j the mass of ion j, $\mathbf{p}_j$ its momentum, q_j its charge, and $\mathbf{A}(\mathbf{r})$ the vector potential corresponding to the magnetic field. We take the direction of the magnetic field as the z direction and we choose $\mathbf{A} = yB_z\mathbf{x}$ where B_z is the magnetic field strength. The total number of ions is given by N. The Hamiltonian due to the electrostatic potential,

$$\hat{H}_\varphi = \sum_{j=1}^{N} q_j \varphi(\mathbf{r}_j) \ , \tag{3}$$

contains the potential due to the end cap electrodes, rotating wall potential, and the Coulomb interaction between the ions, i.e.

$$\varphi(\mathbf{r}) = \frac{1}{2}k_z z^2 - \frac{1}{2}\left(k_x x_r^2 + k_y y_r^2\right) + \frac{1}{4\pi\epsilon_0}\sum_{j=1}^{N}\frac{1}{|\mathbf{r}-\mathbf{r}_j|^2}\ , \tag{4}$$

with ϵ_0 the vacuum permittivity and

$$k_x = \left(\frac{1}{2}+\delta\right)k_z, \qquad k_y = \left(\frac{1}{2}-\delta\right)k_z\ , \tag{5}$$

and

$$\begin{bmatrix} x_r \\ y_r \end{bmatrix} = \begin{bmatrix} \cos(\vartheta(t)) & -\sin(\vartheta(t)) \\ \sin(\vartheta(t)) & \cos(\vartheta(t)) \end{bmatrix}\begin{bmatrix} x \\ y \end{bmatrix} \tag{6}$$

the coordinates of the ions in the frame co-rotating with the wall potential. The phase of the rotating wall potential is

$$\vartheta(t) = \omega_R t + \vartheta_0\ . \tag{7}$$

The Hamiltonian $\hat{H}_L$ describes the radiation pressure forces due to the cooling lasers and is discussed in more detail in section II C.

B. Numerical integration of the motion of the ions

In order to preserve qualitative properties we choose a symplectic integration scheme based on an operator splitting. The general idea is to split the Hamiltonian for the sytem up into pieces that can each be solved exactly. One can then obtain an approximate solution for the time evoluation to the system's dynamics for some time interval Δt by concatenating the time evolution operators for the individual pieces. As a concatenation of symplectic operators this approximate evolution is itself also symplectic. By choosing a time reversal symmetric splitting one obtains an integrator that is accurate to second order in Δt.

In our case we obtain a splitting of the total system Hamiltonian according to the pieces in Eq. 1. The largest frequency in the system is the cyclotron frequency. The splitting in Eq. 1 has the advantage that we account for the cyclotron motion exactly. The remaining pieces in the Hamiltonian only act on the canonical momenta of the particles, i.e. they represent so-called kicks of the particles.

1. *Cyclotron motion*

Fortunately it is elementary to solve the evolution due to the cyclotron motion exactly: The ions move on helical orbits with gyro radius $a_B = mv/(qB)$ with the cyclotron frequency $\omega_B = qB/m$.

2. *Electrostatic Coulomb potential*

The evaluation of the inter-particle interaction is computationally expensive because there are $N(N-1)$ force evaluations required. To do this efficiently we accelerate this step of the computation with GPUs using OpenCL. For the numbers of particles that we're considering here this makes the Coulomb force evaluation approximately 10 times faster than the evaluation of the radiation pressure forces discussed in the next section.

3. $\mathbf{E}\times\mathbf{B}$ *drifts*

As a first test of this integration scheme we demonstrate that it reproduces the $\mathbf{E}\times\mathbf{B}$ drift automatically. This is a useful test because there is a well known solution for the ion motion, see e.g. [**?**]. In addition it illustrates that the concatenation of integratos for cyclotron oscillation with kicks due to the electrostatic potential produces the right overall dynamics which may not be immediately obvious.

To this end we subject an ion to a homogeneous magnetic field along the z direction and a homogeneous electric field along the x direction. The ions react to these fields by drifting along the y direction with a mean velocity

$$v_{\mathbf{E}\times\mathbf{B}} = \frac{\mathbf{E}\times\mathbf{B}}{B^2}\ . \tag{8}$$

The drift of the ions in the y direction is shown in Fig. 1. They move at the correct velocity of $v_{\mathbf{E}\times\mathbf{B}} = 2.2$mm/s. We have checked that the motion perpendicular to both $\mathbf{E}$ and $\mathbf{B}$, i.e. along the z axis in our case, is uniform. Furthermore the period of the cyclotron oscillations and the radius of the cyclotron orbit are correct. Note that the overall features of the cyclotron motion are reproduced accurately even though we are underresolving the cyclotron oscillations by nearly a factor of 10^4: Our time step size is $\Delta t = 1$ms while the cyclotron period is less than 1μs.

This drift is illustrated in Fig. 1. Note that the step size in these simulations was 1ms, approximately 10^4 times larger than the cyclotron period. Nonetheless the drift motion is reproduced accurately.

4. *Convergence of the integrators*

To study the convergence of the integrators we have taken a crystal with 127 ions and prepared them in a steady state by means of artificial cooling... `Need to discuss how we find the stationary state of the ions`

`Make a table of experimental parameters`

We have then integrated the motion of the ions for a total duration of 10μs using various step sizes for the

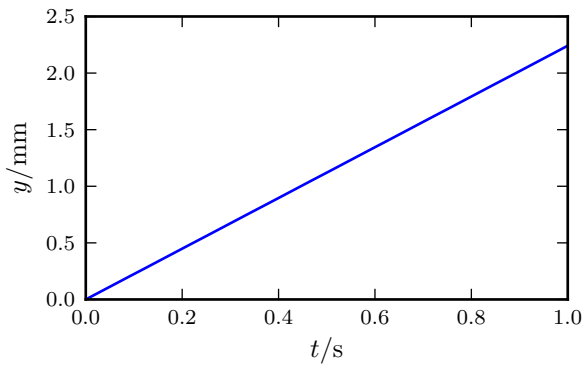

FIG. 1. Drift along y due to crossed magnetic and electric fields.

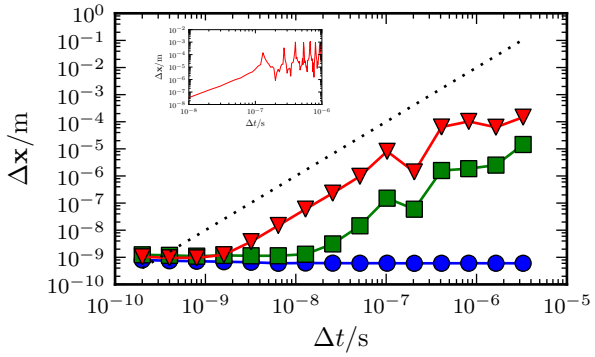

FIG. 2. Convergence of integrators as a function of the time step size Δt. The blue dots show the errors for evolution under the influence of B_z alone. The green squares include the Coulomb repulsion between the ions, and the red triangles include the electrostatic potential. The dashed line has slope 2 and is for orientation. The inset shows a closeup of the errors with magnetic field and Coulomb repulsion in the range $1.0e-8s < \Delta t < 1.0e-6$.

integrator. A reference solution is computed using $\Delta t = 10^{-10}$s. In Fig. 2 we show the mean Euclidean distance between ions in the reference solution and ions for a given Δt,

$$\Delta \mathbf{r} = \sqrt{\frac{1}{N}\sum_{j=1}^{N}(\mathbf{r}_{j,\text{ref.}} - \mathbf{r}_{j,\Delta t})^2}\ . \tag{9}$$

Note that the ion crystal rotates by nearly π radians during $10\mu s$. The ions near the periphery of the crystal travel approximately 1mm during that time. We show the errors for three different cases: evolution under just the magnetic field (blue dots); magnetic field and Coulomb repulsion (green squares); and magnetic field with Coulomb repulsion and electrostatic trap potential. As can be seen, the errors in the solution with just a magnetic field are independent of the time step size up to round-off. Obviously this is to be expected since we solve that part of the problem exactly. When Coulomb repulsion is included the errors are consistent with round-off up to a time step size of $\Delta t \approx 10^{-8}$s. For larger time step sizes the errors grow quadratically. For $\Delta t \approx 10^{-6}$s the errors become comparable to an inter-ion spacing. When the electrostatic potential is included in addition to the Coulomb repulsion the errors are consistent with round-off only up to $\Delta \approx 10^{-9}$s with quadratic growth after that. The errors become comparable to an inter-particle spacing at $\Delta t \approx 10^{-7}$s.

The errors do not grow monotonically once Δt becomes comparable to the cyclotron period $T_{\text{cycl.}} = 1.32 \times 10^{-7}$s. Instead the errors are highly structured as is illustrated in the inset in Fig. 2. This is due to a resonance between the cyclotron motion and the other terms in the Hamiltonian. For instance the first peak in the errors at $\Delta t = T_{\text{cycl.}}$ arises because e.g. the kick due to the electrostatic potential is always applied at the exact same phase of the cyclotron oscillation. Their effects thus add up in a coherent way. The same phenomenon occurs for all harmonics of the cyclotron frequency, i.e. when $\Delta t = nT_{\text{cycl.}}$ with n and integer. In reality the electrostatic potential acts concurrently with the magnetic field during the entire period of the cyclotron oscillations. When the time step size is slightly increased, the kicks are again applied at different phases of the cyclotron motion leading to a more accurate integration.

This observation points to a possible improvement of our integration scheme. The key thing that has to be avoided is a resonance between the cyclotron motion and the kicks. One way to achieve this is by choosing Δt randomly according to a suitably chosen probability distribution. In the present work we do not implement this modification. Instead we use small enough step sizes, $\Delta t \lesssim 10^{-8}$s. The reason for this is two fold. First, for reliable results we need errors that are small compared to an interparticle spacing. Second, larger time steps introduce larger kicks due to laser cooling. These larger kicks cause problems with the crystal stability.

C. Simulation of laser cooling

We adopt a very simplistic model of laser cooling which is directly motivated by the microscopic physics upon which laser cooling based. This model has the advantage of automatically including both deterministic damping as well as the fluctuating forces inherent in laser cooling. Both of these components of the radiation pressure force are required by the fluctuation dissipation theorem. The balance between them gives rise to the Doppler limit.

We model the internal structure of the ions by two quantum mechanical levels representing the two states involved in the cycling transition used for laser cooling. A two level atom at position $\mathbf{r}$ scatters photons out of a laser beam with wavevector $\mathbf{k}$ with a rate

$$\dot{n}(\mathbf{r},\mathbf{v}) = S(\mathbf{r})\frac{\gamma_0}{2\pi}\frac{(\gamma_0/2)^2}{(\gamma_0/2)^2(1+2S(\mathbf{r}))+\Delta^2(\mathbf{v})}\ , \tag{10}$$

where γ_0 is the natural linewidth of the cycling transition (in radians per second), $S(\mathbf{r})$ is the saturation parameter, and $\Delta(\mathbf{v}) = \Delta_0 + \mathbf{k}\cdot\mathbf{v}$ is the detuning of the cooling transition from the laser frequency including the first order Doppler shift. We assume that the atoms scatter photons with this rate with Poissonian number statistics[**?**]. We take into account the beam profile by multiplying the saturation parameter with a Gaussian factor that accounts for the spatial structure of the laser,

$$S(\mathbf{r}) = e^{-\rho^2/\sigma^2} S_0 \ , \tag{11}$$

where ρ is the distance of the atom from the center of the beam and σ is the $1/e$ radius of the intensity of the beam.

To simulate laser cooling we proceed as follows. First we compute the mean number of photons scattered by ion j in time interval Δt,

$$n_j = \dot{n}_j \Delta t \tag{12}$$

The velocities and positions needed for computing $\dot{n}_j$ are taken at the center of the time step in accordance with the integration scheme discussed above. We then compute the actual number of photons scattered by each ion as a Poissonian random number with mean n_j. Each particle receives a total momentum kick of

$$\mathbf{\Delta p}_j = \mathbf{\Delta p}_{\mathbf{j},\text{absorb}} + \mathbf{\Delta p}_{\mathbf{j},\text{emit}} \ , \tag{13}$$

where $\mathbf{\Delta p}_{\mathbf{j},\text{absorb}} = n_j \hbar \mathbf{k}$ and $\mathbf{\Delta p}_{\mathbf{j},\text{emit}}$ is the recoil corresponging to n_j photons scattered in random directions. To compute $\mathbf{\Delta p}_{\mathbf{j},\text{emit}}$ we generate n_j vectors of length $\hbar k$ pointing in random directions. The recoil momentum $\mathbf{\Delta p}_{j,\text{emit}}$ is then obtained by adding up these vectors.

This approach captures the microscopic physics of laser cooling except for two phenomena. First, in the case of strong saturation, $S \gtrsim 1$, quantum statistical phenomena start to play a role. These manifest themselves in the form of anti-bunching of the photons scattered in resonance fluorescence. In essence, there is an anti-correlation between photon emission events due to the fact that immediately after a photon emission an atom is in the ground state with certainty and therefore cannot emitt another photon right away. This correction to resonance fluorescence is probably rather unimportant in the current context, especially because the saturation parameter is not very much greater than 1. The other approximation entering our model is that the photon emission is nearly instantaneous relative to the dynamics of the ions, i.e. the motion is uniform during an excited state lifetime,

$$\eta \equiv T_{\text{cycl}}(\gamma_0/(2\pi)) \ll 1 \ . \tag{14}$$

In our case this ratio is approximately $\eta \sim 0.3$. Furthermore we have to ensure in the simulations that

$$\Delta t \lesssim S\gamma_0/(2\pi) \tag{15}$$

avoid having many photon emission events based on a velocity that was only realized for a small fraction of the time step.

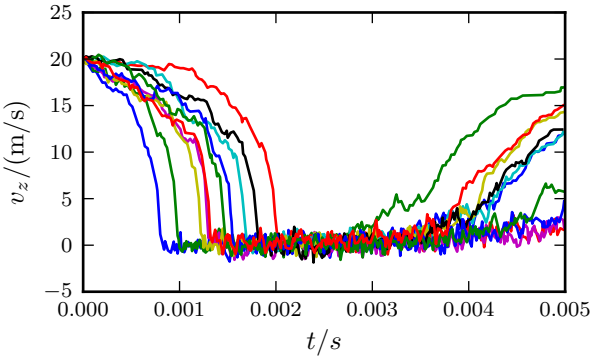

FIG. 3. Velocities of 10 atoms subject to laser cooling. See text for details.

III. FREE SPACE LASER COOLING

As a simple test of our laser cooling model we simulate free space laser cooling, i.e. the ions are not subject to any trapping or magnetic fields. Figure 3 shows the velocities of 10 Be ions subject to laser cooling. The atoms start with a velocity of 20m/s in the positive z direction. Two counter propagating lasers pointed along the z axis irradiate the atoms. The two counter propagating cooling lasers have peak intensities of $S = 0.1$ and are detuned by $0.5\gamma_0$ to the red of the cycling transition at 313nm. The atomic linewidth is $\gamma_0 = 19 \times$ MHz . The laser propagating in the $-z$ direction has a beam waist of 0.01m and the beam propagating in the z direction has a uniform intensity profile (i.e. inifinite beam diameter).

As can be seen in Fig. 3, the ions are cooled to the Doppler limit. Eventually until they diffuse out of the $-z$ beam. After that they are accelerated by the unbalanced power in the z direction. The rms velocity at the Doppler temperature is

$$\sqrt{\langle v_z^2 \rangle} = \frac{\hbar\gamma_0}{3m} \approx 0.25\text{m/s} \ , \tag{16}$$

which is in good agreement with our simulations `Should measure our temperature and calibrate`.

IV. LASER COOLING OF TRAPPED ION CRYSTALS

A. Axial cooling

Figure 3 shows the trajectories of 127 ions subject to axial laser cooling with a saturation parameter of $S = 0.1$.

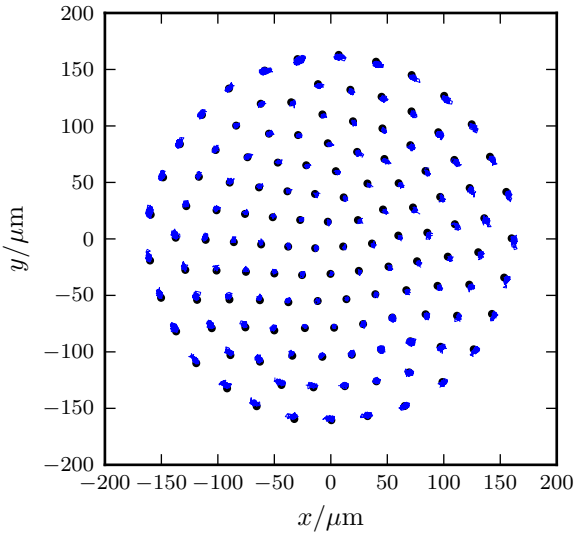

FIG. 4. Top view of ion crystal subject to axial cooling only over a period of 8ms.

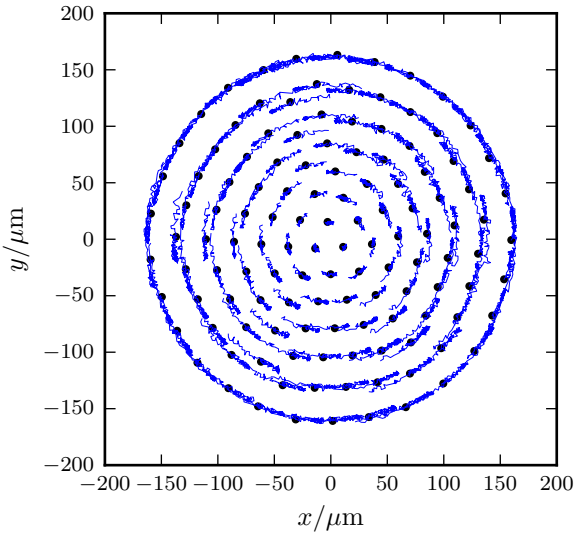

FIG. 5. Top view of ion crystal subject to perpendicular cooling only over a period of 10ms.

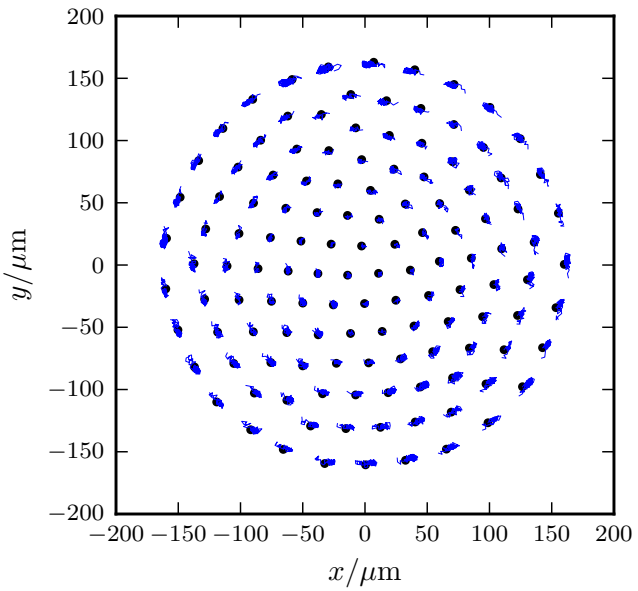

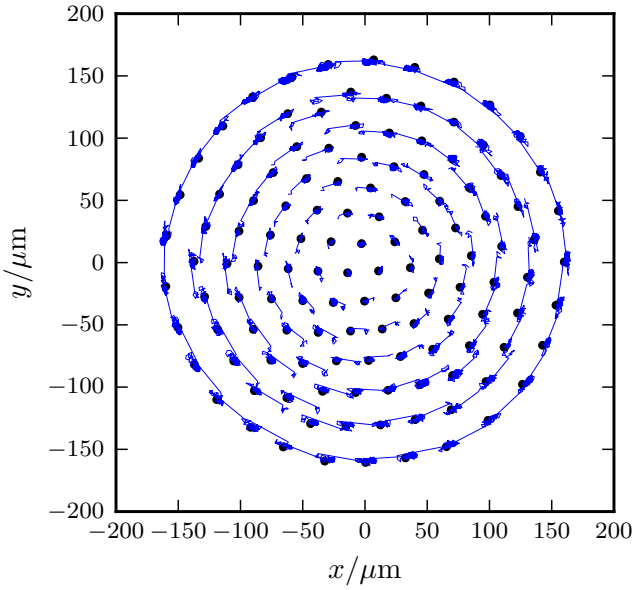

FIG. 6. Top view of ion crystal subject to both perpendicular and axial cooling over a period of 10ms.

B. Perpendicular laser cooling

C. Perpendicular and axial laser cooling

V. FOLLOW UP

It turned out that I had a sign mistake in the rotation frequency of the rotating wall potential. As a consequence the rotating wall potential averaged to zero and I got confinement of the ions merely due to the artificial cooling of their angular motion. This manifested itself in nearly circular ion distributions for trap asymmetries (the parameter δ) for which the crystal should be highly elliptical. In addition I saw large angular drifts (see Fig. 3,4).

After fixing the sign in the rotating wall potential I repeated the numerical experiment where I cool the ion motion with both axial and perpendicular laser cooling. To this end I prepare an initial state using the artificial

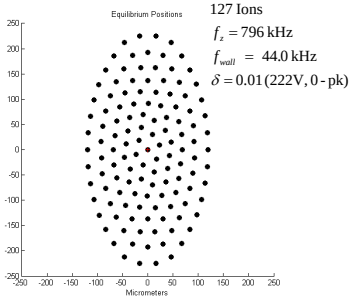

FIG. 7. Stationary crystal configuration as determined by Freericks group's code for 127 ions with $\delta = 0.01$.

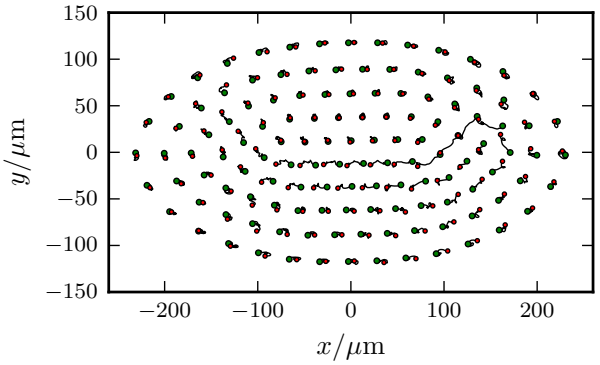

FIG. 8. Dynamics of ion crystal over $1ms$ with parallel and perpendicular laser cooling.

cooling (i.e. without noise and in the rotating frame). I chose a cooling rate for the angular velocity of $\kappa_\theta = 10^8/s$ (i.e. the angular velocity relaxes to the ideal angular velocity $r\omega_W$ with a rate of κ_θ) and $\kappa_z = 10^7/s$ for the axial motion. The rotating wall potential is turned on with $\delta = 0.01$. I have $\omega_W/(2\pi) = 44$kHz and $B = 4.458$T. After about 10ms of evolution with a time step size of $\Delta t = 1$ns the ions settle into an elliptical crystal with an aspect ratio similar to the one predicted by the Freericks group's code, see Fig. 7. There are still some differences between the Freericks ion configuration and the configuration I see in my simulations. For instance the outermost shell contains 32 ions in my simulations while it contains 34 ions in the Freericks calculation. It's possible that my configuration would have settled into the Freericks configuration had I taken the simulations out further. It's also possible that the simulation is stuck in a local energy minimum.

After the initial state has been prepared I switch off the artificial cooling and I switch on the physical laser cooling process described earlier in these notes. Currently this involves writing the simulation state to a file and re-initialize the simulations. A complication with that is that I need to restart the rotating wall potential with the right phase. Otherwise the crystal starts out at an angle with the rotating wall potential. The rotating wall potential then induces large scale coherent motion which is eventually converted into heat. In practical terms this prevents me from getting a crystal.

To avoid this a manually tweak the phase of the wall potential until the crystal and the potential are lined up with one another. The intial state of the crystal at this point in the simulations is indicated by the green dots in Fig. 8.

I follow the dynamics of the ions for a total of 1ms with a time step size of $\Delta t = 1$ns. The path that the ions trace out during this time is indicated by the black lines. The final positions are indicated by the red dots. The dynamics is somewhat easier to understand by looking at a movie. Two horizontal lines of ions just below the center of the crystal start moving to the left. Eventually a few ions take up the vacencies generated by moving an entire inter particle spacing. They eventually end up in the starting positions of their neighbouring ions. This whole process takes almost 1 ms. It involves collective motion of the ions. Each ion by itself cannot move much. Instead several ions have to cooperate in order to find a lower energy state.

Note that with the sign of the rotating wall potential fixed the ion crystal is rather stationary in the rotating frame. I do not see the large overall drifts anymore.

This simulation took about 1.5h on my laptop. I'm hoping to tweak the various parameters for the numerical integration to make this go faster. There are several low hanging fruits in terms of optimization. In terms of physics I'd like to look at smaller values of δ as discussed per email. I'd also like to repeat the numerical experiment with only parallel cooling or only perpendicular cooling. Then there is the experiment of moving the perpendicular cooling laser off center. Presumably these will require that I take the simulations out further.

- Laser cooling derives from mechanical effects of light in the course of resonance fluorescence.
- Model it in a stochastic way.
- Because the ions have a large velocity spread in the lab frame due to the rotation of the crystal we have to account for large Doppler shifts. Take realistic lineshape into account.
- Probability for photon scattering given by
- This is appropriate if the excited state lifetime is short compared to the cyclotron period. This is not exactly fulfilled in our case. We have to improve on this in the future. E.g. stochastic wavefunction trajectories.
- This gives rise to damping, radiation pressure forces (torque on crystal) and fluctuations, all of which are

important for the static and dynamic properties of the crystals.

- Validation Look at free space cooling, reproduce Doppler temperature
- Validation: Look at axial temperature of ions in trap. Both agree.

A. Convergence of the integration scheme

In figure **??** I show the convergence of our integrator as a function of the time step size. That figure shows the mean error in the position of 400 ions after $0.1ms$. This corresponds to several periods of the rotating wall potential. The trap parameters are the same as in Fig. **??**. The ions are propagated until steady state is reached. From that point on we integrate for another 0.1ms with varying step sizes.

VI. STATIC CRYSTAL ANALYSIS

This is mostly validation work, i.e. trying to convince ourselves that we're getting things right by comparing against well understood experimental data and Freericks group's theory.

A. Aspect ratio as a function of rotating wall potential strength

B. 1-2 plane transition

C. Crystal symmetry

VII. PHONON DYNAMICS, SPECTRA, TEMPERATURES, ETC.

A. Spectra

- Comparison with Freericks group.
- Excitation level, $< n_i >$, etc.
- Mode structure

VIII. STABILITY OF CRYSTAL

- Excursions of ions as a function of perp cooling beam width, displacement from trap center; can do this spatially resolved (i.e. are certain regions of the crystal "hotter" than others)
- Frequency of rearrangements; nature of rearrangements.

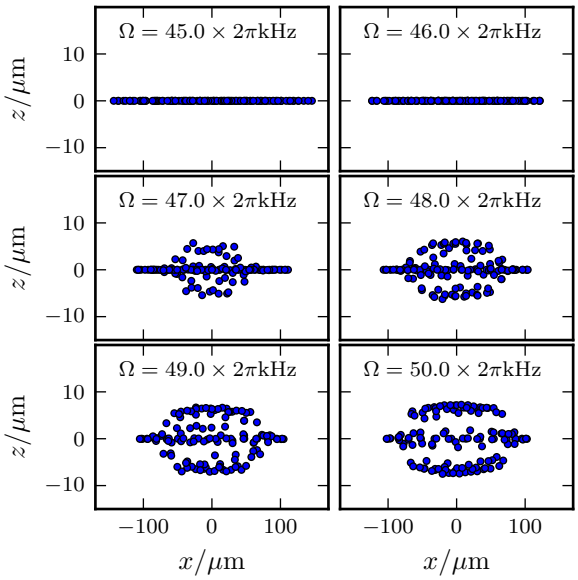

FIG. 9. Side view of the ions in steady state for different rotation frequencies. At $\Omega \approx 50 \times 2\pi$kHz the single plane configuration becomes unstable.

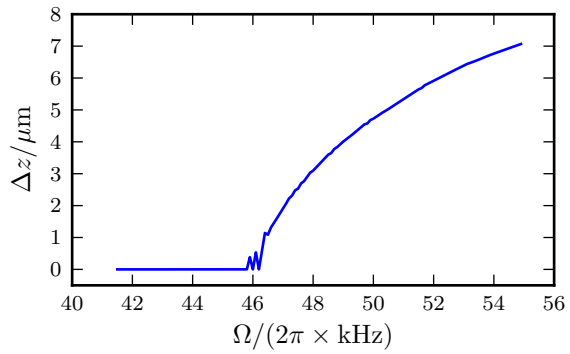

FIG. 10. Thickness of the ion crystal as a function of Ω

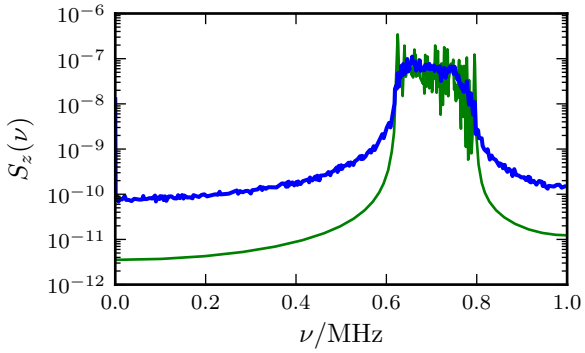

FIG. 11. Axial spectra. The green line is without cooling and the blue line is with continuous cooling during the recording of the spectrum.

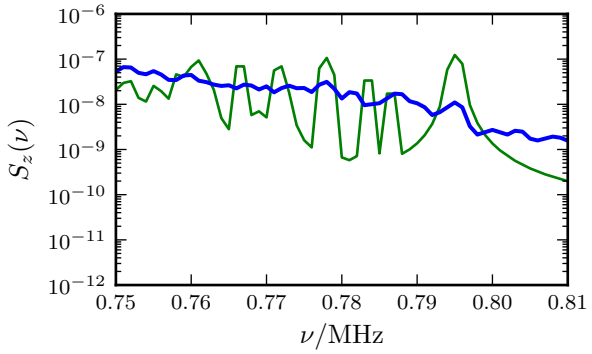

FIG. 12. Axial spectra. The green line is without cooling and the blue line is with continuous cooling during the recording of the spectrum. The highest modes (especially the com mode) are visible.

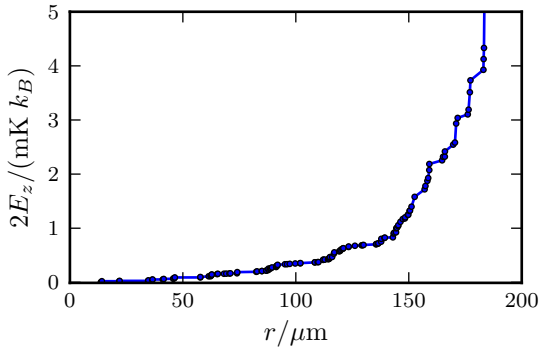

FIG. 13. Axial temperature as a function of disctance from center of crystal.

IX. INVESTIGATE OTHER COOLING CONFIGURATIONS

- E.g. counterpropagating cooling beams

X. CONCLUSION